Looped finger transformation in frustrated cholesteric liquid crystals

J. Baudry, S. Pirkl,* and P. Oswald
Laboratoire de Physique,† ENS Lyon, 46 Allée d'Italie, 69364 Lyon Cedex 07, France
(Received 16 October 1998)

Localized structures named ''fingers'' form in the vicinity of the unwinding transition of a cholesteric liquid crystal subjected to an electric field and to homeotropic boundary conditions. Several types of fingers exist, with different static and dynamic properties. For instance, cholesteric fingers of the second species (CF-2) can drift perpendicular to their axes and form spirals in ac electric fields, whereas fingers of the first species (CF-1) crawl along their axes. In this article we show that CF-2's are much easier to nucleate in thick samples (with respect to the pitch) than in thin ones and may form loops like the CF-1's, with or without defects. We show that looped CF-1's always collapse in thick samples at increasing voltage, whereas they can form cholesteric bubbles in thin samples. By contrast, we never observe the formation of a bubble from a loop of a CF-2 except when it possesses a point defect. We also recall that CF-1 segments always collapse at increasing voltage, whereas CF-2 segments systematically give cholesteric bubbles in similar conditions. To qualitatively explain these transformations, we use a simplified representation on the unit sphere $S2$ of the director field within the fingers. While the CF-1's are described within the standard model of Press and Arrot, we use for the CF-2's a recent model of Gil and Gilli, which we prove to explain most observations. We also describe the growth and collapse dynamics of a loop of a CF-2 in close connection with the spiral dynamics. Finally, we show experimentally and numerically that the CF-2's get abruptly thinner when the electric field exceeds the spinodal limit of the CF-1's. This transformation is reversible, but strongly hysteretic.
[S1063-651X(99)08205-7]

PACS number(s): 61.30.Gd, 61.30.Jf, 47.20.Ky

I. INTRODUCTION

During the last ten years, many experiments have been devoted to the problem of the unwinding transition of a cholesteric liquid crystal in confined geometry [1–30]. In standard experiments, the sample is sandwiched between two parallel ITO electrodes which are treated in homeotropic anchoring. These boundary conditions are topologically incompatible with the helical structure of the phase, which, consequently, unwinds if the sample thickness is too small. In practice, the control parameter is the confinement ratio $C=d/p$ of the thickness over the equilibrium pitch. The transition to the homeotropic nematic phase takes place when $C\leqslant C_c=K_{32}/2$, where K_{32} is the ratio K_3/K_2 (the K_i's are the usual Frank constants of the cholesteric phase) [3]. Another way to unwind the helix is to use a liquid crystal of positive dielectric anisotropy ε_a and to apply a voltage V between the two electrodes. This control parameter is much easier to vary than the thickness.

So, in practice, the thickness is fixed and the voltage is changed. In this way it is possible to show that the transition is usually first order [10]. In particular, there exists a voltage V_2 where the two phases coexist. More precisely, V_2 is the voltage for which the cholesteric fingers of the first species (CF-1's) have exactly the same energy as the nematic. At this voltage, a segment of a CF-1 has a constant length. The CF-1's have been known for a long time because they are the most easy to obtain experimentally. Nevertheless, other kinds of fingers exist near V_2, which can be nucleated in special conditions, for example, at the cholesteric-isotropic interface in directional growth [29]. The most interesting are the cholesteric fingers of the second species (CF-2's) because they can drift and form spirals in ac electric fields, contrary to CF-1's. In the microscope they look very similar to the CF-1's, which explains why both types of fingers have often been confused.

There also exist in the samples other objects of circular shape, named cholesteric bubbles [31–35]. These bubbles have been known for a long time and form spontaneously at the cholesteric-isotropic transition. Another way to produce a bubble is to shrink in electric field a looped CF-1 [35] or a segment of a CF-2 [22].

In this article, we show the possibility to form looped CF-2's. Depending on the value and on the frequency of the electric field, these loops grow or collapse, but never form bubbles contrary to CF-1's, except when they have a point defect. This feature is certainly connected to the topology of the CF-2. In addition, we study the growth and collapse dynamics of looped CF-2's in close connection with the formation of spirals. Finally, we show that the CF-2's abruptly get thinner when the applied voltage exceeds the spinodal limit V_3 of the CF-1, a phenomenon that can be theoretically explained from the Gil-Gilli model of Ref. [30].

II. EXPERIMENTAL SETUP AND PHASE DIAGRAM

The sample is obtained by mixing the liquid crystal 5 CB (4-n-pentyl-4′-cyanobiphenyl) with 3.25 wt % of the chiral molecule CB15 (from Merck Corp.). The cholesteric pitch is measured in a Cano wedge and equals 4.5 μm at 30 °C. The sample is prepared between two parallel ITO electrodes

*Permanent address: Department of Physics, University of Pardubice, 53210 Pardubice, Czech Republic.
†Associé au CNRS, UMR 8514.

 ©1999 The American Physical Society

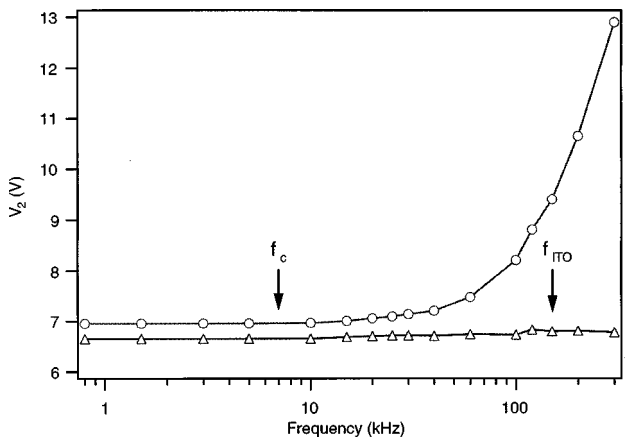

FIG. 1. Voltage V_2 for the fingers of the first species (in volt rms) as a function of the frequency ($C=4.44$). Curve 1 (circles) corresponds to the voltage which is applied between the two electrodes; curve 2 (triangles) is the voltage which is really applied to the cholesteric sample.

treated with silane ZLI 3124 from Merck to obtain a strong homeotropic anchoring. The sample thickness is fixed with Mylar spacers or nickel wires of calibrated thicknesses or diameters. We performed most of our experiments with a 20-μm-thick sample, which gives a confinement ratio of $C \approx 4.44$. This is a pretty large value compared to our previous experiments: this choice will be justified in the following. For comparison, we also did experiments in thinner samples ($C=1.78$, 2.22, and 3.33). All our observations and measurements are done at 30 °C. At this temperature $K_1 \approx K_3$ in 5CB [36], which makes easier our numerical simulations (see Sec. VII).

A square-wave ac voltage is applied between the two electrodes. In order to characterize the sample, we first measured as a function of the frequency the coexistence voltage V_2 for the CF-1's. At this voltage, the fingers have the same energy as the nematic phase, and consequently do not grow or shorten. In Fig. 1, we plot V_2 as a function of the frequency in the thick sample ($C=4.44$). Two curves are shown. The first one is the voltage which is applied between the two electrodes: it strongly increases at high frequency, typically when $f>100$ kHz. A similar effect was already reported without clear explanation by Mitov and Sixou [17]. It is in fact an artifact which is due to the voltage decrease across the two ITO layers. Indeed, these two layers act as a resistance R_{ITO}, which is in series with the sample, and the one can be modeled by a resistance R_s in parallel with a capacity C_s. From these three constants, two characteristic frequencies can be constructed: the charge relaxation frequency of the sample $f_c=(R_sC_s)^{-1}$ and another frequency $f_{\mathrm{ITO}}=(R_{\mathrm{ITO}}C_s)^{-1}$ that depends on the ITO layer. As a result, the voltage that is really applied to the sample (V_2^{samp}) must be different from that experimentally measured (V_2^{expt}). This voltage can be easily calculated providing that R_{ITO}, R_s, and C_s are known. We measured these three constants (which we found to be independent of the frequency up to 300 kHz) with a precision *LCR* meter HP4284A, which allowed us to calculate V_2^{samp}. This voltage is displayed in Fig. 1: we note that it is constant and does not change significantly when we go from the conducting regime ($f<f_c$) to the dielectric one ($f>f_c$) ($f_c \approx 7$ kHz in this sample); by contrast, the measured voltage V_2^{expt} significantly shifts from V_2^{samp} at high frequency when $f>f_{\mathrm{ITO}} \gg f_c$ ($f_{\mathrm{ITO}} \approx 150$ kHz). Because most of our experiments were performed at frequencies $f<f_{\mathrm{ITO}}$, we will be aware of this correction in the following. Finally, we observed that the sample heats when the frequency exceeds f_{ITO} because of the Joule effect. The temperature increase ΔT is estimated by measuring the shift to the melting temperature. Negligible at 40 kHz (of the order of 0.1 °C), it becomes important above f_{ITO} (for instance, $\Delta T \approx 0.95$ °C at $f=300$ kHz). In order to maintain constant the sample temperature, we systematically decreased of ΔT the temperature of the oven above 40 kHz.

TABLE I. $V_2 \approx V_2^*$ are the coexistence voltages for the fingers of the first and of the second species; V_3 (V_3^b) defines the spinodal limit for the CF-1's (the bubbles); V_{tr}^* ($\approx V_3$) is the voltage above which the CF-2's get abruptly thinner; V_{rtr}^* ($\approx V_2$) is the voltage below which the thin CF-2 recovers its initial width; V_{ltr} is the voltage above which a looped CF-1 transforms into a bubble (†) or collapses. The asterisk (*) refers to the CF-2's.

$C=d/p$	1.78	2.22	3.33	4.44
V_2	3.23	3.96	5.28	7.0
V_2^*	3.28	3.96	5.28	7.0
V_3	4.02	4.8	6.05	7.7
V_3^b	3.92	4.64	5.99	7.46
V_{tr}^*	4.04	4.85	6.05	7.59
V_{rtr}^*	3.88	4.34	5.26	7.01
V_{ltr}	3.64†	4.40	5.81	7.3

We then measured the coexistence voltage V_2^* for the CF-2's, and we found that $V_2 \approx V_2^*$ in all samples except the thinnest one in which V_2^* is slightly larger than V_2 (this is in good agreement with previous measurements [25]). We also measured the spinodal limits V_3 and V_3^b for the CF-1's and the bubbles, respectively. We found that V_3^b is slightly smaller than V_3 contrary to what we previously observed in thinner samples (in which $C<1.6$ [35]). That means that the cholesteric bubbles are more stable in thin samples than in thick ones.

All these data are reported in Table I as a function of the confinement ratio $C=d/p$ at $f=5$ kHz.

III. SEGMENTS AND LOOPS OF FINGERS OF THE FIRST AND SECOND SPECIES: COLLAPSE OR TRANSFORMATION INTO CHOLESTERIC BUBBLES

Let us first consider segments of a CF-1 and a CF-2. We know from previous experiments that the former have two different tips (a pointed one and a rounded one), whereas the latter have almost similar rounded tips. More important, the former systematically collapse above V_2, whereas the latter systematically form bubbles above V_2^* (and below V_3^b) [22]. These transformations are shown in Fig. 2. We also recall that a CF-2 segment may easily extend below V_2 (rigorously below a voltage V_n that is a little bit smaller than V_2 [25]) by forming two segments of a CF-1. In this case, there exists a point defect at each junction between the CF-2 and CF-1's.

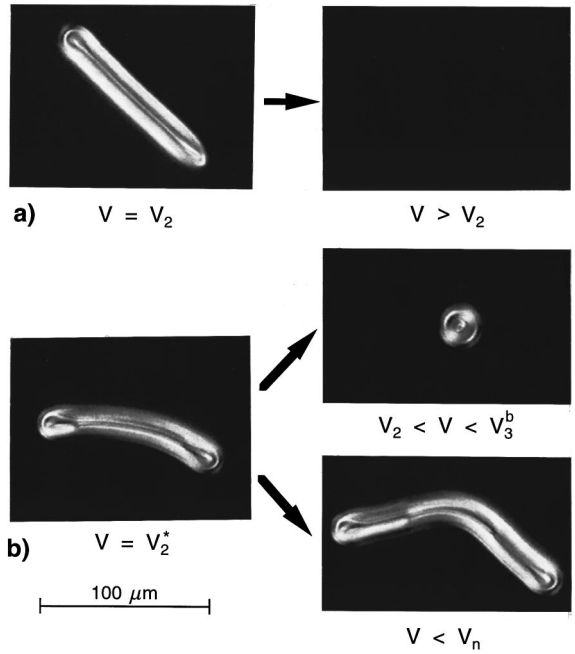

FIG. 2. (a) Segment of a CF-1. It collapses above V_2. (b) Segment of a CF-2. It gives a bubble above V_2^*, while it lengthens by forming two CF-1 segments with similar rounded tips below V_n ($C=3.38$, $p=14.8\ \mu$m, $f=5$ kHz, $V_2=5.02$ V).

In addition, the two CF-1 segments end with similar rounded tips (Fig. 2).

Second, we consider loops of these fingers.

We already showed that a loop of a CF-1 may transform into a bubble if the voltage is large enough (in practice, larger than V_2, but smaller than V_3^b) [35]. During this irreversible transformation, the core of the loop collapses, whereas its external ring shrinks to form the bubble (Fig. 3). This transformation only occurs in thin samples (typically when $C<2$). When $C>2$, the loops collapse without forming bubbles. Typical values of the voltage V_{ltr} above which a CF-1 loop transforms into a bubble or collapses are given in Table I.

Similarly, it was possible for the first time to form loops of a CF-2. Such loops are much easier to obtain in large-d/p samples than in thin ones. Indeed, the CF-2's nucleate as easily as the CF-1's in thick samples (typically $C>3$) when electrically ''quenching'' the sample from the nematic phase into the finger region. In Fig. 4(a), we show such a loop: optically, it looks like a CF-1 loop and a simple observation through the microscope is not sufficient to distinguish them. By contrast, we shall see in the following section that their dynamic behaviors are quite different and allow us to distinguish them without ambiguity. As for the CF-1 loops, it was possible to shrink them by increasing the voltage while remaining in the domain of existence of the bubbles. We observed that the CF-2 loops always collapse without giving bubbles. Nevertheless, we failed to make a CF-2 loop without defects in the thinnest sample ($d/p=1.78$) in which we observed the transformation of a CF-1 loop into a bubble. On the other hand, it was possible to make CF-2 loops containing one point defect. In this case, the loops systematically transform into bubbles [Fig. 4(b)]. In fact, looped CF-2's with one or several defects spontaneously form in all the samples. For instance, we show in Fig. 5 a loop with four point defects. By increasing the voltage close to V_3^b, this loop breaks at the places of the defects and give four segments of a CF-2, which then form four bubbles.

In the following section, we describe the dynamical properties of the looped CF-2's.

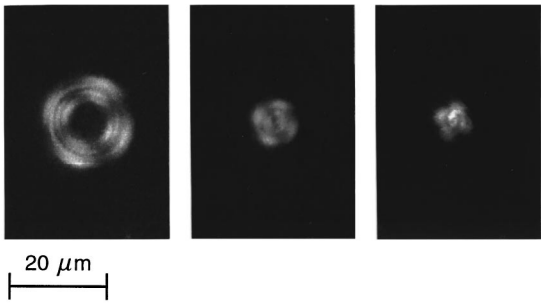

FIG. 3. A looped CF-1 may form a bubble in thin samples ($C=1.68$, $V=7.6$ V, $f=20$ kHz).

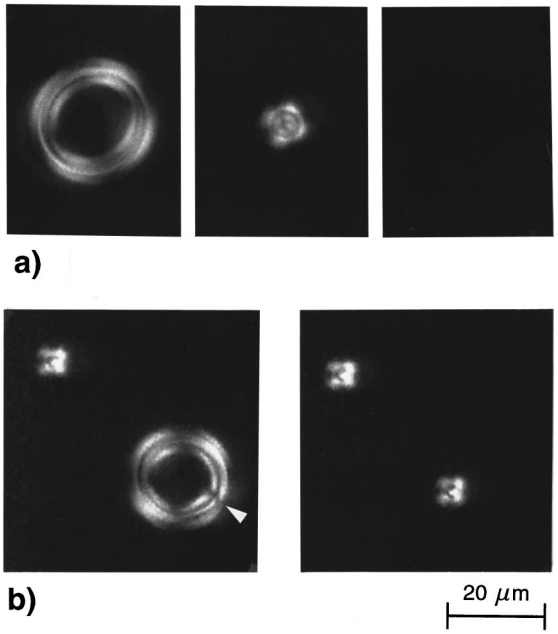

FIG. 4. (a) A looped CF-2 without defect always collapses above V_{tr}^* ($V=7.6$ V, $f=5$ kHz, $C=4.44$). (b) A looped CF-2 containing one point defect always transforms into a bubble above V_{tr}^* ($V=7.6$ V, $f=20$ kHz, $C=4.44$).

IV. DYNAMIC PROPERTIES OF LOOPED CF-2's

We know from previous experiments [14–18,22,25] that the CF-2's form spirals in ac electric fields when one at least of their two ends are free to move (Fig. 6). These spirals spontaneously form close to V_2^* because the fingers drift perpendicularly to their axes providing the frequency is not too large ($f<f_c$ [37]). In Ref. [25], we showed that the spiral tends to an Archimedian spiral far from its center, where the finger drifts at constant velocity ν_0. This velocity is given as a function of the frequency in Fig. 7.

Let us now consider a looped CF-2. At a voltage larger than V_2^*, the experiment shows that there is a critical radius

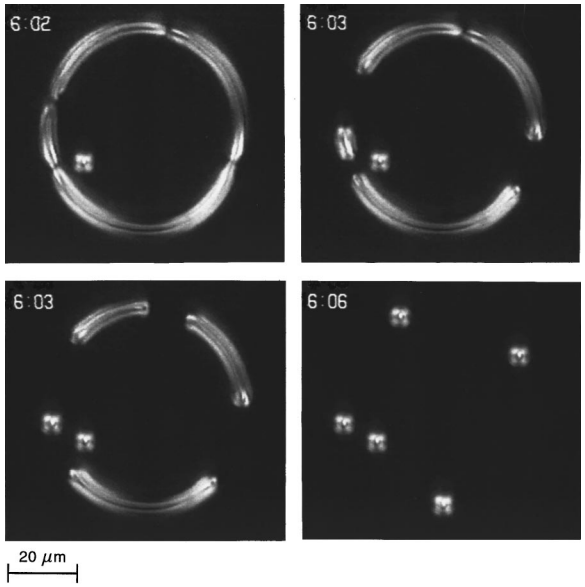

FIG. 5. Loop of a CF-2 with four point defects. Above V_{tr}^* this loop breaks at the places of the defects to form four segments which finally will give four bubbles ($V=7.6$ V, $f=20$ kHz, $C=4.44$).

R_c below which the loop collapses and above which it grows. In Fig. 8, we report the radius of the loop as a function of time for different initial radii R_i. To explain the loop dynamics, we consider the forces that act on the finger. There is an outward driving force F_e which opposes to two inward forces: the viscous force F_v, which we assume to be proportional to the velocity ($F_v=\nu_{\text{drift}}/m$) and the line tension force proportional to the line energy T and inversely proportional to the finger radius of curvature R. Balancing these three forces, we get

$$\nu_{\text{drift}}=\frac{dR}{dt}=m\left(F_e-\frac{T}{R}\right), \tag{1}$$

where m is a mobility inversely proportional to the rotational viscosity γ_1. The line tension T is assumed constant, i.e., independent of R, which means that we neglect the curvature energy of the finger. This assumption is valid if

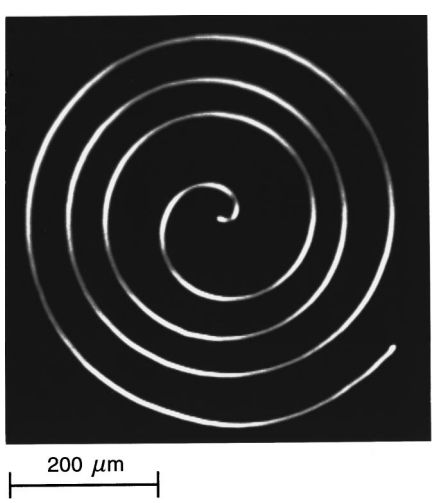

FIG. 6. Archimedian spiral of a CF-2 observed in the thick sample ($C=4.44$, $V=7.2$ V, $f=5$ kHz).

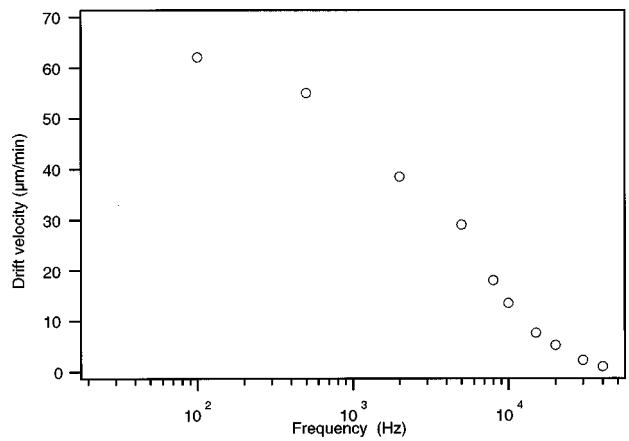

FIG. 7. Asymptotic drift velocity ν_0 of a CF-2 as a function of the frequency at $V=V_2^*$ ($C=4.44$).

$\Delta V=V-V_2^*$ is large enough in order that the line energy of the rectilinear finger T (which is proportional to ΔV: see Sec. VII and Fig. 18) is much larger than its curvature energy. In thick samples ($C\approx 3$), the cholesteric helix is almost not deformed except near the two glass plates and the finger is equivalent to a cholesteric layer of thickness p (see Fig. 16). The bend energy of such a layer has been calculated by Chandrasekhar [38] and equals $(3/8)K_3 dp/R^2$. Moreover, we have calculated numerically the line energy of a CF-2 as a function of the applied voltage: $T\approx 11K_1\Delta V$ (see Sec. VII and Fig. 18). Experimentally, we performed all our measurements at $\Delta V>0.5$ V. In these conditions, the curvature energy of the fingers can be neglected as long as

$$R\gg\sqrt{\frac{3}{88}\frac{C}{\Delta V}}p$$
$$\approx 2.5\ \mu\text{m}\quad\text{by taking}\quad C=4.44\quad\text{and}\quad p=4.5\ \mu\text{m}. \tag{2}$$

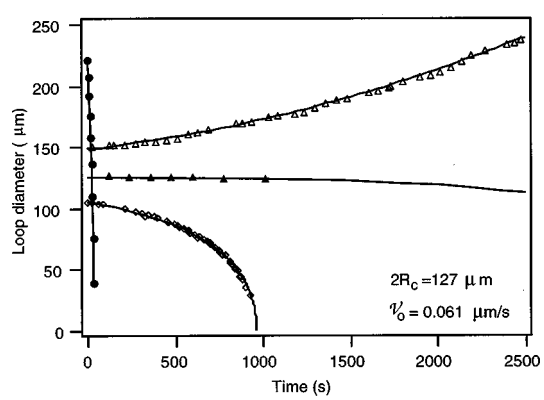

FIG. 8. Radius of a loop of a CF-2 as a function of time for different initial radii R_i. When $R_i<R_c$, the loop collapses, whereas it grows when $R_i>R_c$ ($V=8$ V, $f=25$ kHz, $C=4.44$). The three solid line curves are fitted to Eq. (3) by adjusting R_c and ν_0. The asymptotic velocity ν_0 is equal to that measured from the spirals ($\nu_0=0.06\ \mu$m/s). The critical radius R_c of the loop depends on the voltage and frequency as shown in Fig. 9. For comparison, we also plotted in this graph the time evolution (solid circles) of a transformed loop at $V=8$ V, $f=25$ kHz, and $C=4.44$.

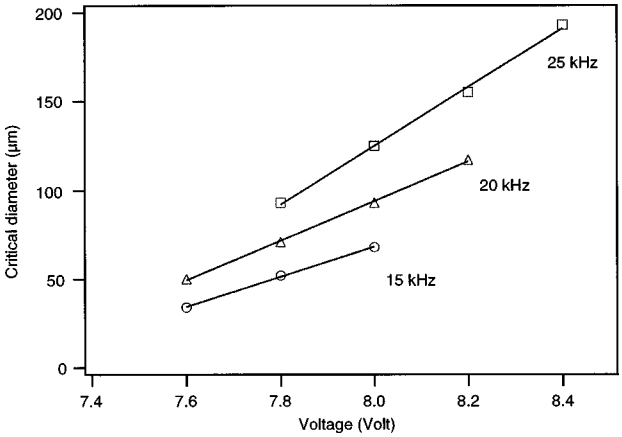

FIG. 9. Critical radius of looped CF-2's as a function of the voltage at three different frequencies ($C=4.44$). Extrapolation of the lines show that R_c vanishes at 7.2 V (respectively, 7.16 and 7.24 V) when $f=15$ kHz (respectively, 20 and 25 kHz). These values are equal to V_2^* within experimental errors (see Fig. 1).

This condition being fulfilled experimentally (see Figs. 8 and 9), we shall neglect the curvature energy of the finger in the following. Integration of Eq. (1) (with T constant) gives

$$\nu_0 t=(R-R_i)+R_c \ln\left(\frac{R-R_c}{R_i-R_c}\right), \tag{3}$$

with

$$R_c=\frac{T}{F_e}. \tag{4}$$

In Fig. 8 we fit the experimental curves to Eq. (3) by adjusting R_c and ν_0. We found $\nu_0=0.061\ \mu$m/s, in good agreement with the value found experimentally at the same frequency for the drift velocity of a spiraling finger [ν_0(spiral)$=0.059\ \mu$m/s].

Finally, we measured the critical radius of the looped CF-2's as a function of the voltage at three different frequencies. These data, given in Fig. 9, show that the critical radius is proportional to V and vanishes at V_2^*:

$$R_c \alpha (V-V_2^*). \tag{5}$$

This behavior is quite compatible with Eq. (4) inasmuch as the line energy T vanishes at V_2^*, by definition.

V. TOPOLOGICAL MODEL AND CONSTRUCTION ON THE UNIT SPHERE $S2$

In 1976, Press and Arrott proposed a model for describing the cholesteric fingers of the first species [5,6]. In their model, the director field is numerically calculated by assuming that all the elastic constants are equal (isotropic elasticity). It was shown later that the unwinding transition must be second order in these conditions [10], which is not observed experimentally. To explain why the transition is first order, elastic anisotropy must be taken into account, a refinement that does not change the topology of the CF-1's [10]. The corresponding director field $\mathbf{n}(x,y,z)$ is shown in Fig. 10(a).

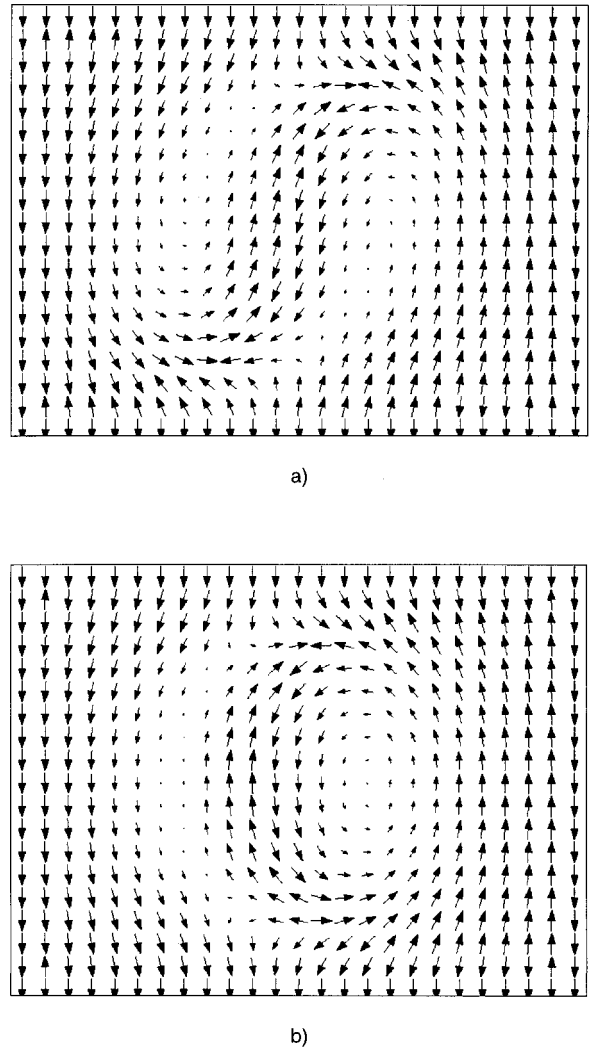

FIG. 10. (a) Director field inside a cross section of a CF-1 (after the model of Press and Arrott [4,5]). (b) The same for a CF-2 (after the model of Gil and Gilli [30]). This finger can be simply obtained from a CF-1 configuration by rotating of π about the z axis of the lower half part of the finger. This operation requires the helix to be perfect in the middle plane of the sample.

As noted by Gil and Thiberge [28], a CF-1 satisfies the following symmetry:

$$n_{y,z}^{\text{CF-1}}(-y,-z)=\varepsilon n_{y,z}^{\text{CF-1}}(y,z),$$

$$n_x^{\text{CF-1}}(-y,-z)=-\varepsilon n_x^{\text{CF-1}}(y,z) \quad (\varepsilon=\pm 1). \tag{6}$$

Because of the $\mathbf{n}\rightarrow-\mathbf{n}$ invariance, this symmetry implies that the CF-1 is invariant by a π rotation around the x axis (parallel to the finger axis). The z axis is perpendicular to the glass plates. As a consequence, the CF-1 does not drift perpendicularly to its axis in ac electric fields [28].

By contrast, the CF-2 drifts in ac electric fields and gives spirals and growing loops at $V>V_2^*$. An explanation proposed by Gil and Gilli [30] would be that a CF-2 drifts with different velocities according to whether the electric field is up or down. This is possible if the finger is not invariant by a π rotation around the x axis. The continuous director field of Fig. 10(b) found numerically by Gil and Gilli satisfies

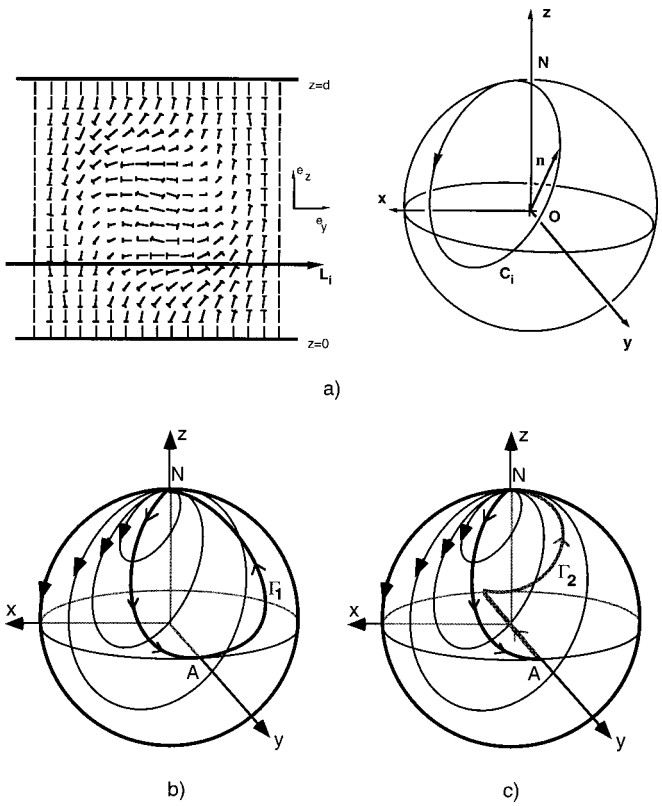

FIG. 11. Representation on the unit sphere $S2$ of the director field within the fingers. Each circle C_i on $S2$ represents the trajectory of the director along a line L_i of the real space (a). In a CF-1 the centers of the circles C_i describe a closed curve Γ_1, which is, thus, continuously reducible to the north pole (b). By contrast, the corresponding curve Γ_2 in a CF-2 is open and cannot be continuously reduced to the north pole (c).

these conditions and so could describe the CF-2. In this case, the Lehman effect could be the motor of the drift, but this interpretation has still to be confirmed experimentally.

In the following we show that the topological model of Gil and Gilli is compatible with our observations.

To simplify, we propose to represent the director field on the unit sphere $S2$ [39]. This method proved to be very useful in cholesterics [40,41], in particular for explaining most properties of the CF-1's and of their phase diagram [10–14,27]. The idea is to associate with the director at a point of the real space, a point on $S2$. In this representation, the image of the director along a line in the real space is a trajectory on $S2$. By convention, the north pole N corresponds to the homeotropic orientation. Also two diametrically opposite points are equivalent because of the $\mathbf{n}\rightarrow-\mathbf{n}$ invariance. To represent a finger (supposed invariant along the x axis), we consider the images of all the straight lines parallel to the y axis that intersect the finger. Because of the homeotropic boundary conditions, the corresponding trajectories on $S2$ are closed curves C going from N to N. It was previously shown [10,27] that these trajectories may be approximated to circles [Fig. 11(a)].

We now describe the two types of fingers. On $S2$, each finger is represented by a set of circles C. Let Γ be the trajectory of their centers on $S2$.

In a CF-1, Γ is a *closed* curve Γ_1 going from N to N [Fig. 11(b)]. In this case, the finger can be continuously reduced to the north pole. This explains why the CF-1's easily nucleate from the nematic phase when the electric field is reduced.

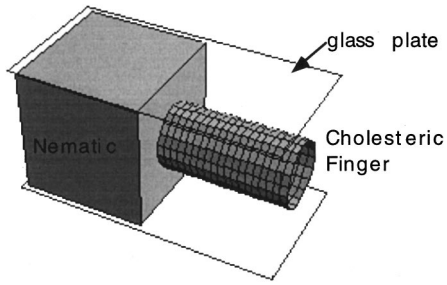

FIG. 12. Cube surrounding a finger end.

By contrast, Γ is no longer a closed curve in a CF-2 [Fig. 11(c)]. Indeed, circles C now cover the whole sphere $S2$ so that Γ_2 is composed of two arcs of a circle, NA and BN, which are symmetric with respect to the NS axis of $S2$ (S is the south pole). In this representation, A and B are diametrically opposed and equivalent because they are the centers of the same grand circle on $S2$. But we now see that the director field is no longer reducible to the north pole via a continuous transformation. This explains the exceptional resistance of the CF-2's to an increasing electric field (see Fig. 8 of Ref. [22] and Sec. VI).

This representation on $S2$ is also very useful to predict whether there exist point defects at the ends of a finger. The simplest way to answer this question is to consider a cube surrounding the end of a finger (Fig. 12) and to count how many times the image P on $S2$ of the director $\mathbf{n}$ covers the whole sphere while moving around the cube. This integer N defines the topological rank of the point defect ($N=1,2,\ldots$) [42]. Note that $N=0$ if there is no defect (in this case, P does not completely describe $S2$). By using the representation on $S2$ of the fingers, it is immediate to check that $N=0$ in each end of a CF-1, whereas $N=1$ in each end of a CF-2.

As a consequence, a CF-1 segment is continuous, which we have known for a long time. By contrast, there exists a point defect of rank $N=1$ in each end of a CF-2 segment. These defects are visible in the microscope and subsist when two CF-1 segments prolong the CF-2 [Fig. 2(b)]. These defects are not centered in the sample as can be easily seen by superimposing the director fields of Figs. 10(a) and 10(b). In this case, two possibilities must be considered, depending on whether the two tips of the two CF-2's are different or not (this depends on the orientation chosen for the CF-2 with respect to the CF-1 when one superimposes the two director fields). In the former case, the two point defects are identical and lie at the same height in the sample (while being closer to one plate than to the other). In the latter case, which is indeed experimentally observed for energetical reasons (rounded tips are less energetical than the sharp ones [8,11,14]), the two defects lie at different heights in the sample, which can be seen in the microscope by changing the focus. This observation may explain the formation of a bubble with two point defects along its axis (see the topological model of Ref. [35]) when the CF-2 shortens. Finally, we observed in a very thick sample ($d=50\,\mu$m and $p=14.8\,\mu$m) that these two point defects can move along the finger (providing it is long enough), meet, and change sides

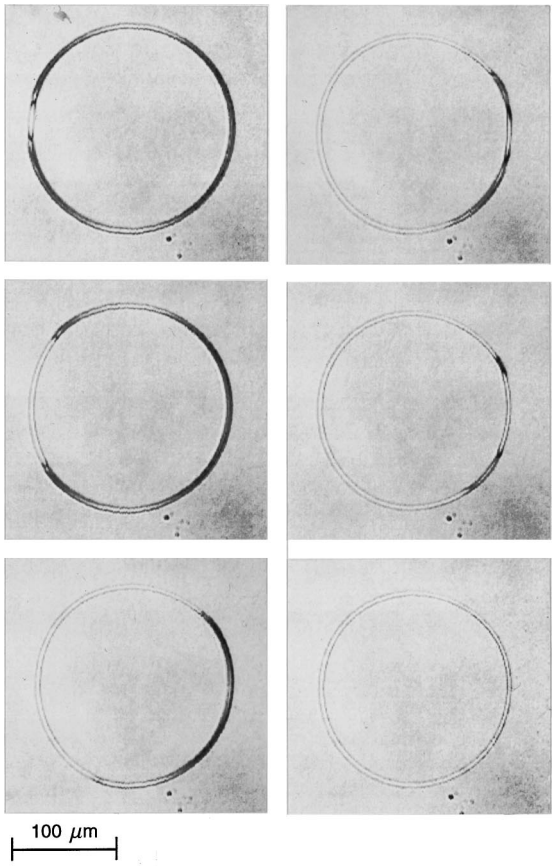

FIG. 13. Transformation of a loop of a CF-2 at $V=V_{tr}^{*}=8.45$ V, $f=25$ kHz, and $C=4.44$ (unpolarized light). The finger locally pinches off, generating pairs of solitons which propagate along the fingers. Each soliton separates two regions of different widths and optical contrasts.

without visible interaction. It is interesting to note that after crossing, the curvature of the CF-2 segment has changed sign. Such a finger, when it shortens, gives a bubble, however, as in other samples.

VI. TRANSFORMATION OF THE CF-2's IN HIGH ELECTRIC FIELDS

The behavior and optical contrast of the CF-2's change when the applied voltage exceeds a well-defined voltage V_{tr} (Figs. 13 and 14). At this voltage, which is very close to the spinodal limit V_3 of the CF-2's (see Table I), the fingers abruptly become thinner while their optical contrast decreases (Fig. 14). This transformation is not homogeneous at V_{tr}, but proceeds from the nucleation and propagation along the loop axis of pairs of ''solitons'' which form at each elementary ''stricture.'' After the transformation, all these ''solitons'' disappear (Fig. 13). By contrast, this transformation looks homogeneous if the voltage is abruptly switched to a voltage a few hundredths of a volt above V_{tr}^{*}. This transformation of the CF-2 was observed in all the samples and was systematically observed at a voltage very close to V_3 (see Table I). A direct consequence of this transformation is a brutal change of the dynamic properties of the loop. Indeed, they usually start to quickly collapse immediately after the transformation, whereas they were growing just before. This effect is shown in Fig. 8 in which the radius of a transformed loop is displayed as a function of time. On the other hand, we observed that the transformed loop can grow if its radius is larger than some critical radius R_c^{+}, which turns out to be much larger than that R_c of the initial loop. This is shown in Fig. 15 where both critical radii are reported for comparison at different frequencies.

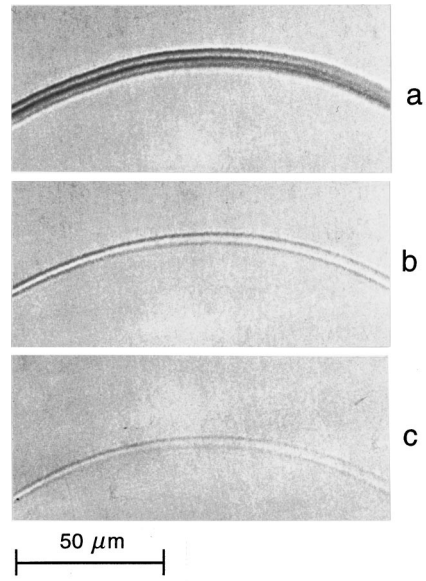

FIG. 14. Part of a CF-2 loop observed at large magnification before (a) and after transformation (b), (c) ($C=4.44$, $f=25$ kHz, unpolarized light). (a) $V=8$ V, (b) $V=8.5$ V, and (c) $V=10$ V. By increasing the voltage, the apparent width as well as the optical contrast of the finger decreases, suggesting it also becomes thinner within the sample thickness.

Finally, we observed that this transformation is reversible if the voltage is decreased below a voltage V_{rtr}^{*} which is very close to V_2^{*} (see Table I). This transformation is thus strongly hysteretic.

VII. ENERGETICAL MODEL

In order to explain our observations, we numerically calculated the director field and the energy per unit length of the

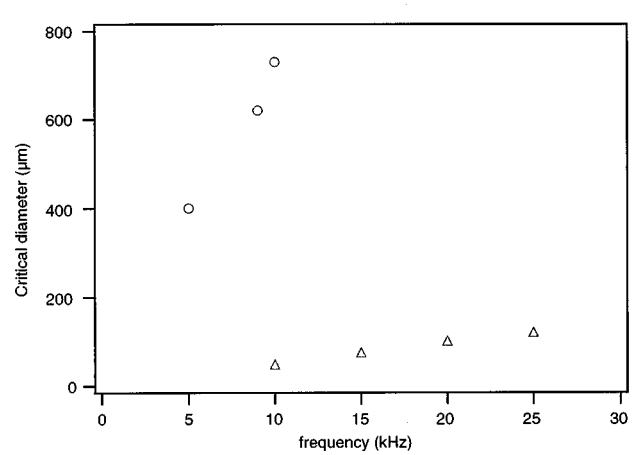

FIG. 15. Critical radii R_c (triangles) and R_c^{+} (circles) of looped CF-2's before and after transformation as a function of the frequency. At high frequency, R_c^{+} becomes so large that it becomes impossible to measure ($C=4.44$, $V=7.8$ V).

two types of finger (supposed to be invariant along the x axis). In practice, we must solve the differential equations

$$\frac{\delta f}{\delta n_i}=\frac{\partial f}{\partial n_i}-\frac{\partial}{\partial y}\frac{\partial f}{\partial n_{i,y}}-\frac{\partial}{\partial z}\frac{\partial f}{\partial n_{i,z}}=0, \tag{7}$$

where f is the Frank energy

$$f=\frac{1}{2}K_1(\mathrm{div}\,\mathbf{n})^2+\frac{1}{2}K_2(\mathbf{n}\cdot\mathrm{curl}\,\mathbf{n}+q)^2 + \frac{1}{2}K_3(\mathbf{n}\times\mathrm{curl}\,\mathbf{n})^2-\frac{1}{2}(\mathbf{D}\cdot\mathbf{E})^2 \tag{8}$$

(with $q=2\pi/p$), together with the Maxwell equation giving the local electric field [29]:

$$-\frac{\delta f}{\delta V}=\mathrm{div}\,\mathbf{D}=0, \tag{9}$$

where $\mathbf{D}=(\varepsilon)\mathbf{E}$. This equation is only valid in the dielectric regime ($f>f_c$). In the conducting regime ($f<f_c$), the equation

$$\mathrm{div}\,\mathbf{j}=0, \tag{10}$$

with $\mathbf{j}=(\sigma)\mathbf{E}$, must be solved instead of Eq. (9).

In practice, we did our calculations using Eq. (9). Nevertheless, we checked that the value of V_2 numerically found depends very little (within 1%) on the condition chosen (although the spatial distribution of the electric field within the sample be quite different). This result is in agreement with the experiment (see Fig. 1).

A relaxation method is used, consisting in solving the equations

$$\frac{\partial n_i}{\partial t}=-\frac{\delta f}{\delta n_i} \tag{11}$$

and

$$\frac{\partial V}{\partial t}=-\frac{\delta f}{\delta V}. \tag{12}$$

In order to satisfy the normalization condition $n^2=1$, we project at each step of the calculation the elementary displacement $\delta n_i=-(\delta f/\delta n_i)\delta t$ onto the sphere $n^2=1$ [24]. The finger energy is then calculated by integrating f over a cross section of the finger. Our initial configurations for the CF-1's and CF-2's are that given by the geometrical model of the circles on $S2$ (see Sec. V). Finally, we did our calculations by taking $K_1=K_3=3.5\times10^{-7}$ dyn, $K_2=1.6\times10^{-7}$ dyn [36], $\varepsilon_\parallel=16.2$ and $\varepsilon_\perp=7.3$ [43]. These values are those given in the literature for pure 5CB, 3 °C below its clearing temperature.

Let us first discuss the results concerning the CF-1's. As a typical example, we show the director field and shift of the vertical component E_z of the electric field from its mean value V/d in Fig. 16 when $C=3.33$ and $V=3.92$ V. In Table II, we give the values of V_2 and V_3 calculated at $C=2.22$. We recall that the finger has the same energy as the nematic phase at V_2, whereas above V_3 the finger spontaneously disappears. We also give in Table II the theoretical value of V_0 calculated from the exact formula [3,11,14]

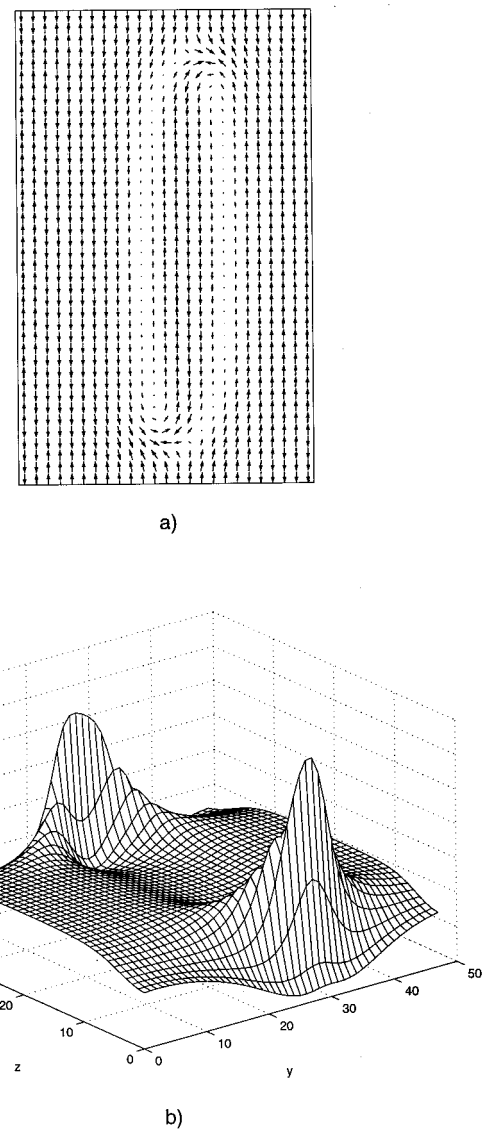

FIG. 16. Director field in a cross section of a CF-1 (a) and the deviation of the vertical component of local electric field from its mean value V/d (b) ($C=3.33$, $V=3.92$ V).

$$V_0=\sqrt{-\frac{K_{32}}{4A}+\frac{C^2}{K_{32}A}}\quad\text{with}\quad A=\frac{\varepsilon_a}{4\pi^2K_2}. \tag{13}$$

TABLE II. Values of the different voltages obtained at $C=2.22$.

	V_0	V_2	V_2^*	V_{tr}^*	V_{rtr}^*
Experimental	2.05	3.96	3.96	4.85	4.34
Numerics	1.17	2.23	2.23	2.95	2.6

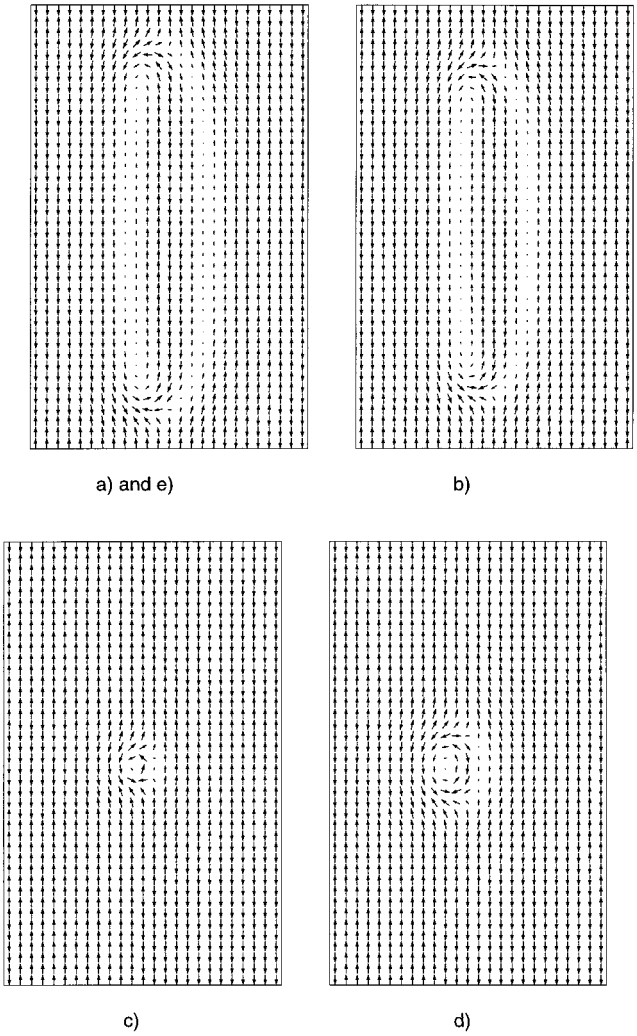

FIG. 17. Director field in a cross section of a CF-2 calculated at $C=3.33$ by first slowly increasing the voltage [(a) $V=3.92$ V, (b) $V=4.37$ V, (c) $V=4.4$ V], and then by slowly decreasing the voltage [(d) $V=3.95$ V, (e) $V=3.92$ V]. The energy of these fingers is given in Fig. 18.

We note that there is a constant factor of the order of 1.7 between calculated and measured values. One possible explanation for this discrepancy is discussed in the next section.

Similarly, we have computed the director field inside a CF-2 as a function of the applied voltage (Fig. 17). As expected, the CF-2 does not disappear when the voltage increases. On the other hand, its width abruptly decreases when the applied voltage exceeds a voltage V_{tr}^* we found very close to V_3. This is not surprising inasmuch as the director field of a CF-2 close to one plate is quite similar to that of a CF-1 at large thickness ($C \gg 1$). By decreasing the voltage, we numerically observed that the finger remains very thin down to a voltage V_{rtr}^* intermediate between V_2 and V_3. This hysteretic behavior is observed experimentally (see Sec. VI). We also calculated V_2^* for the CF-2's, and we found that $V_2=V_2^*$ at large C, again in very good agreement with the experiment. Values of V_2, V_2^*, V_{tr}^*, and V_{rtr}^* are reported in Table II at $C=2.22$.

Finally, we plot in Fig. 18 the energy (with respect to the nematic phase) of the two types of fingers as a function of the applied voltage. As expected in thick samples, the two types of fingers have the same energy below V_3. Above V_3, the CF-1's collapse, whereas the CF-2's get abruptly thinner. This new solution corresponds to the upper branch of the diagram. The CF-2's stay on this branch when the voltage is decreased down to V_{rtr}^*. Below, they recover their ''normal'' width corresponding to the lower branch of the diagram.

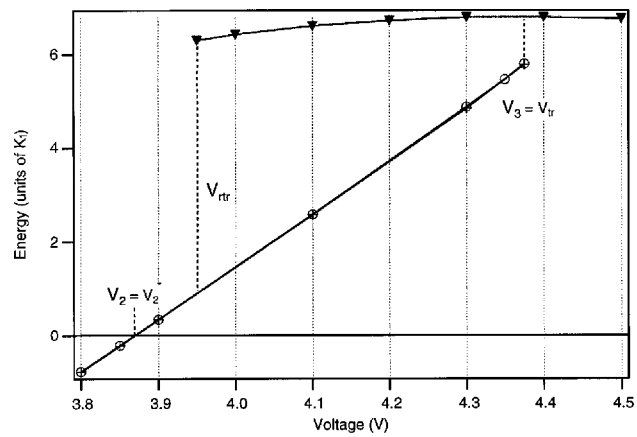

FIG. 18. Energies in units of K_1 (with respect to the nematic phase, assumed to be 0) of the CF-1's (circles) and of the CF-2's as a function of the voltage V at $C=3.33$ before transformation (crosses) and after transformation (triangles).

VIII. CONCLUDING REMARKS

We have seen that there is only a qualitative agreement between theory and experiments inasmuch as the measured voltages are systematically larger by a factor of 1.6–1.7 than the calculated ones (see Table II). The explanation for this discrepancy is that the values of the elastic constants and dielectric anisotropy at a given temperature (30 °C in our experiment) change with respect to those of pure 5CB when chiral molecules are introduced (in our experiment we add 3.25 wt % of CB15 to the sample, which causes a decrease of the melting temperature from 34.2 °C down to 31.5 °C). This interpretation is reinforced by the fact that the agreement is better at small concentration. For instance, we found that at $C=1.7$, $V_0(\text{theory})=0.9$ V [calculated from Eq. (13) by using the values of the pure 5CB at 30 °C], whereas experimentally, at the same temperature, $V_0(\text{expt})=1.2$ V when $p=15\,\mu$m (0.98 wt % of chiral molecules) and $V_0(\text{expt})=2$ V when $p=4.5\,\mu$m (3.21 wt % of chiral molecules). Note that in the sample with 0.98 wt % of CB15, the melting temperature only decreases by 0.8 °C.

ACKNOWLEDGMENTS

This work was supported by the European Research Network ''Pattern Noise and Chaos in Complex Systems'' under Contract No. FMRX-CT96-0085, and by the Barrande Program between France and the Czech Republic under Contract No. 98010.

[1] P. Cladis and M. Kléman, Mol. Cryst. Liq. Cryst. **16**, 1 (1972).
[2] Finkelmann H. Brehm and H. Stegemeyer, Ber. Bunsenges. Phys. Chem. **78**, 883 (1974).
[3] W. Greubel, Appl. Phys. Lett. **25**, 5 (1974).
[4] M. J. Press and A. S. Arrott, J. Phys. (Paris) **37**, 387 (1976).
[5] M. J. Press and A. S. Arrott, Mol. Cryst. Liq. Cryst. **37**, 81 (1976).
[6] T. Harvey, Mol. Cryst. Liq. Cryst. **34**, 224 (1978).
[7] M. Kawachi, O. Kogure, and K. Kato, Jpn. J. Appl. Phys. **17**, 391 (1978).
[8] A. Stieb, J. Phys. (Paris) **41**, 961 (1980).
[9] P. Oswald, J. Bechhoefer, and A. Libchaber, Phys. Rev. A **36**, 5832 (1987).
[10] F. Lequeux, P. Oswald, and J. Bechhoefer, Phys. Rev. A **40**, 3974 (1989).
[11] P. Ribière and P. Oswald, J. Phys. (Paris) **51**, 1703 (1990).
[12] S. Pirkl, Cryst. Res. Technol. **26**, K111 (1991).
[13] P. Ribière, S. Pirkl, and P. Oswald, Phys. Rev. A **44**, 8198 (1991).
[14] P. Ribière, Ph.D. thesis, Université Claude Bernard-Lyon I, 1992.
[15] J. M. Gilli and M. Kamayé, Liq. Cryst. **11**, 791 (1992).
[16] J. M. Gilli and M. Kamayé, Liq. Cryst. **12**, 545 (1992).
[17] M. Mitov and P. Sixou, J. Phys. II **2**, 1659 (1992).
[18] M. Mitov and P. Sixou, Mol. Cryst. Liq. Cryst. **231**, 11 (1993).
[19] S. Pirkl, Cryst. Res. Technol. **28**, 1027 (1993).
[20] T. Frisch, L. Gil, and J. M. Gilli, Phys. Rev. E **48**, R4199 (1993).
[21] P. Ribière, S. Pirkl, and P. Oswald, Liq. Cryst. **16**, 203 (1994).
[22] P. Ribière, P. Oswald, and S. Pirkl, J. Phys. II **4**, 127 (1994).
[23] J. M. Gilli and L. Gil, Liq. Cryst. **17**, 1 (1994).
[24] L. Gil, J. Phys. II **5**, 1819 (1995).
[25] S. Pirkl and P. Oswald, J. Phys. II **6**, 355 (1996).
[26] T. Nagaya, Y. Hikita, H. Orihara, and Y. Ishibashi, J. Phys. Soc. Jpn. **65**, 2707 (1996).
[27] T. Nagaya, Y. Hikita, H. Orihara, and Y. Ishibashi, J. Phys. Soc. Jpn. **65**, 2713 (1996).
[28] L. Gil and S. Thiberge, J. Phys. II **7**, 1499 (1997).
[29] J. Baudry, S. Pirkl, and P. Oswald, Phys. Rev. E **57**, 3038 (1998).
[30] L. Gil and J. M. Gilli, Phys. Rev. Lett. **80**, 5742 (1998).
[31] M. Kawachi, O. Kogure, and Y. Kato, Jpn. J. Appl. Phys. **13**, 1457 (1974).
[32] W. E. L. Haas and J. E. Adams, Appl. Phys. Lett. **25**, 263 (1974); **25**, 535 (1974).
[33] N. Nawa and K. Nakamura, Jpn. J. Appl. Phys. **17**, 219 (1978).
[34] S. Hirata, T. Akahane, and T. Tako, Mol. Cryst. Liq. Cryst. **38**, 47 (1981).
[35] S. Pirkl, P. Ribière, and P. Oswald, Liq. Cryst. **13**, 413 (1993).
[36] N. V. Madhusudana and R. Pratibha, Mol. Cryst. Liq. Cryst. **89**, 249 (1982).
[37] J. Baudry, S. Pirkl, and P. Oswald (unpublished).
[38] S. Chandrasekhar, *Liquid Crystals*, 2nd ed. (Cambridge University Press, Cambridge, England, 1992).
[39] R. N. Thurston and J. Almgren, J. Phys. (Paris) **42**, 413 (1981).
[40] F. Lequeux, Ph.D. thesis, Orsay University, 1988.
[41] F. Lequeux, J. Phys. (Paris) **49**, 254 (1988).
[42] E. A. Dubrovin, S. P. Novikov, and A. E. Fomenko, *Modern Geometry: Methods and Applications* (Springer, New York, 1990), Pts. I–III.
[43] B. R. Ratna and R. Shashidhar, Mol. Cryst. Liq. Cryst. **42**, 113 (1977).